

1 A Fast Detection Method for Wheat Mould Based on Biophotons

2

3 Short title: Fast Detection for Wheat Mould by Biophotons

4

5 Gong Yue-hong¹, Yang Tie-jun¹, Liang Yi-tao¹, Ge Hong-yi^{1,2}, Chen Liang³

6

7 ¹ School of Information Science and Engineering, Henan University of Technology, Zhengzhou,

8 China

9 ² Key Laboratory of Grain Information Processing & Control, Ministry of Education, Henan

10 University of Technology, Zhengzhou, China

11 ³ College of Biological Engineering, Henan University of Technology, Zhengzhou, China

12

13 * Corresponding author

14 E-mail: tjyanghlyu@126.com

16

17 **Abstract**

18 Mould is a common phenomenon in stored wheat. First, mould will decrease the quality
19 of wheat kernels. Second, the mycotoxins metabolized by mycetes are very harmful for humans.
20 Therefore, the fast and accurate examination of wheat mould is vitally important to evaluating its
21 storage quality and subsequent processing safety. Existing methods for examining wheat mould
22 mainly rely on chemical methods, which always involve complex and long pretreatment
23 processes, and the auxiliary chemical materials used in these methods may pollute our
24 environment. To improve the determination of wheat mould, this paper proposed a type of green
25 and nondestructive determination method based on biophotons. The specific implementation
26 process is as follows: first, the ultra-weak luminescence between healthy and mouldy wheat
27 samples are measured repeatedly by a biophotonic analyser, and then, the approximate entropy
28 and multiscale approximate entropy are separately introduced as the main classification features.
29 Finally, the classification performances have been tested using the support vector
30 machine(SVM). The ROC curve of the newly established classification model shows that the
31 highest recognition rate can reach 93.6%, which shows that our proposed classification model is
32 feasible and promising for detecting wheat mould.

33

34

35

36

37

38

39 Introduction

40 Wheat, as a type of global grain, is one of the staple foods that human beings and animals
41 rely on throughout the world. The history of wheat cultivation can be traced back to ten thousand
42 years ago, and it has become the second most cultivated crop in the world due to its high
43 productivity and strong adaptability [1]. As the world population has increased over the last
44 decade, the consumption of wheat has also increased [2], which can be seen in Fig. 1.

45 **Fig. 1. Global Consumption of Wheat and Year-on-Year Percentage from 2009 to 2018.**

46 When a suitable surrounding moisture and temperature is achieved, microorganisms
47 make great contributions to the wheat mould phenomenon, thus affecting the quality and quantity
48 of stored wheat [3]. Since mould is inevitable during the wheat storage period, the health of
49 human beings will be extremely threatened once certain edible food that is made using mouldy
50 wheat as raw materials are available in their daily lives [4]. Many mycotoxins are metabolized by
51 mouldy wheat, among which aflatoxin B1 (AFB1) is the most striking contaminant and has the
52 strongest carcinogenicity [5]. Nearly one quarter of crops in the world are contaminated by
53 aflatoxins before or during their storage period according to the Food and Agriculture
54 Organization (FAO). Once feeds and foods are made of mouldy kernels, the AFB1 carried within
55 will cause a series of illnesses, such as retarded growth, immune suppression, human or animal
56 death, and so on [6]. Therefore, the development of fast and green techniques for detecting AFB1
57 in stored wheat kernels is very necessary to ensure human and animal safety.

58 The study of biological photons can be traced to 1923 when the Russian biologist
59 Gurwitsch used biological detectors to test the roots of onions and found a special phenomenon:
60 onion cells can produce faint light that can stimulate other cells to accelerate their cell division
61 [7]. The Italian scientist Coli placed some plant buds on detectors with photomultiplier tubes for

62 measurement and observed an ultra-weak light emission phenomenon [8]. In the later 1970s, led
63 by West German physicians, biophoton research conducted many experiments and made striking
64 progress [9]. In the 1980s, biophoton technology was applied to spontaneously detect various
65 plant seeds, including wheat, celery, soybean, and others, and obtained fruitful achievements.
66 Subsequently, the scientific team represented by Veselova analysed in detail the quality and
67 performance of various crop seeds (soybean, barley, sunflower, etc.) using the delayed radiation
68 of biophotons and found that there is a negative correlation between seed vigour and a delayed
69 luminescence signal [10]. In recent decades, the research of biophoton technology has made
70 tremendous development. A large number of experiments have proved that biophoton radiation
71 is a common life phenomenon that is related to biological and physiological activities, the
72 generation and synthetization of DNA, and other information exchange or energy transmission
73 processes. The higher the level of an organism is, the greater intensity of the photon radiation
74 that is emitted. The research applying of biophoton technology has been mainly conducted in
75 medical fields, such as medical information diagnosis [11], cancer classification [12], analysis of
76 brain activities [13], and others. In the cereal storage field, however, biophoton studies mainly
77 focus on insect intrusion rather than on wheat mould. Duan et al. [14] have applied the
78 permutation entropy algorithm to analyse the biophoton signals of wheat kernels and then use a
79 BP network to test the experimental effects. Their proposed algorithm not only improves the
80 detection rate by 10% but also saves the sample training time [14]. Regarding the detection
81 process of insect intrusion, spontaneous biophoton emission, which is also known as ultra-weak
82 luminescence (UWL), has been proven to be a sensitive index at reflecting the mould among
83 wheat kernels. The main achievements in this paper are that we have measured the UWL of
84 healthy and mouldy wheat kernels separately using biophotonic technology, calculated the

85 approximate entropy and multiscale approximate entropy as the main classification parameters,
86 and then, we used the SVM to test the classification performance of newly established model.

87

88 **Materials and methods**

89

90 **Materials**

91

92 **Wheat kernel samples**

93 The experimental wheat kernels were offered by the Yuda grain barn, Zhumadian city,
94 Henan Province in 2019. Some pretreatment, such as finding foreign materials and imperfect or
95 damaged kernels, washing the kernels several times using distilled water, drying the samples to a
96 certain degree of moisture using special equipment and so on, is very necessary. Subsequently,
97 the wheat sample is divided into two parts: one is the healthy samples, and the other part is sent
98 to the College of Biological Engineering to cultivate the mould in the sample with 50%
99 *Aspergillus flavus*. Regarding the healthy wheat samples, we prepared 240 subsamples weighing
100 20.00 ± 0.01 g. We use 120 subsamples as the training group (experimental group), and the
101 remaining 120 subsamples form the testing group. Regarding the mouldy wheat samples, 120
102 subsamples are used as the training group, and the other 120 subsamples are used as the testing
103 group. Meanwhile, protective measures should be taken during this process due to the strong
104 poisonous of AFB1.

105

106 **Equipment**

107 The BPCL-2-ZL, manufactured by Beijing Jianxin Lituo Technology Co., Ltd., was used
108 to measure the biophotons of healthy and mouldy wheat samples.

109 Fig. 2 shows the whole analysis system, which consists of three parts: ① a detection
110 chamber, where the tested samples are input; ② a biophoton analyser, mainly including the
111 photon counting and optical hi-voltage converter device; and ③ computer equipment, which
112 displays results from the corresponding software on a monitor. The calculated average
113 background noise of the instrument is 28 counts per second, The high voltage for the test is set as
114 1030 V, and the testing temperature is $25.0\pm 0.5^{\circ}\text{C}$.

115 **Fig. 2. Instrumentation Used in the Experiment.**

116

117 **Methods**

118 The whole detection process consists of two parts. One part is selecting the right
119 environmental parameters. Since the experimental result may be influenced by surrounding
120 factors, all the experiments should be conducted under the same conditions to minimize the
121 environmental influences, including the same environmental temperature ($20\pm 1^{\circ}\text{C}$), humidity
122 ($25\pm 6\%$), and measuring time (8:00 am~18:30 pm). The other part is choosing suitable
123 experimental parameters. Before testing, each sample was placed for 30 min in a dark space to
124 decrease the interference from ambient parasitic light. Since the spontaneous biophotonic
125 radiation of wheat kernels is not strong enough, the sampling interval is set to 10 s in order to
126 collect ample numbers of biophotons. To better reflect the properties of the UWL signals of the
127 two types of wheat samples, the total sampling time is extended over 15,000 s. Then, the UWL
128 signals of the healthy and mouldy wheat kernel samples are measured separately.

129 **Results**

130

131 **Biophotonic data analysis**

132 One hundred and twenty groups of healthy and mouldy wheat samples were measured by
133 the above processes. Owing to the nonlinear and random characteristics of the number of
134 biophotons, we calculated the average numbers of photons for all the samples for both types, and
135 the results are shown in Fig. 3. Table 1 shows their statistical characteristics, such as the mean,
136 variance and standard deviation. As Table 1 shows, the statistical biophotonic characteristics of
137 mouldy wheat are larger than those of healthy wheat. This difference occurs because the
138 *Aspergillus* fungi that colonized the wheat kernels have much stronger metabolism and
139 respiration. The large number of biophotons in mouldy wheat also provides a convincing
140 explanation, which coincides with physiological regularity such that the higher the level of an
141 organism is, the greater the intensity of the biophotons it emits.

142 **Fig. 3. Average UWL Data of Healthy and Mouldy Wheat.**

143 **Table 1. UWL Data Statistical Characteristics of Two Types of Wheat.**

	Mouldy wheat kernels in 2019	Healthy wheat kernels in 2019
Mean	84.22	71.11
Variance	5830.37	3533.45
Standard deviation	76.36	59.44

144 To effectively distinguish between healthy wheat and mouldy wheat based on UWL data,
145 we will use the approximate entropy (ApEn) and multiscale approximate entropy (MApEn)
146 algorithm, and then comparing their performances.

147

148 **Approximate entropy**

149 The approximate entropy (ApEn) algorithm was proposed by the scholar Pincus to
150 measure the characteristics of random series [15]. The more complex an initial time series is, the
151 larger its corresponding ApEn. The ApEn is suitable for analysing the biophoton signals of
152 wheat kernels because of its more robust performance. Two prominent advantages of the ApEn
153 are its lower dependency on the length of the initial time series and strong resistance to the noise
154 contained in the original data.

155 The complete computing process of the ApEn is [16]:

156 Divide the original series $X = \{x(i), i = 1, 2, \dots, N\}$ into an m -dimensional vector $u(i)$,
157 which is shown as follows:

$$158 \quad u(i) = \{x(i), x(i+1), \dots, x(i+m-1)\}, i = 1, 2, \dots, N-m+1 \quad (1)$$

159 Here, m represents the dimension of the pattern vector, and N denotes the initial length
160 of the time series.

161 1) Calculate the distance $d[u(i), u(j)]$ between vector $u(i)$ and vector $u(j)$ using formula 2.

$$162 \quad d[u(i), u(j)] = \max_{k=0,1,\dots,m-1} |x(i+k) - x(j+k)| \quad (2)$$

163 2) Count the numbers of $d[u(i), u(j)] < r$, where r , which is known as the similar tolerance
164 threshold value, is a positive real number. Then, calculate the proportion between

165 $d[u(i), u(j)] < r$ and the total number of vectors, which is labelled as $C_i^m(r)$ in equation 3.

$$166 \quad C_i^m(r) = (\text{number of } d[u(i), u(j)] < r) / (N - m + 1) \quad (3)$$

167 1) Calculate the logarithm of $C_i^m(r)$, and then, obtain its mean using equation 4. Here, the

168 mean is labelled as $H^m(r)$.

$$169 \quad H^m(r) = \frac{1}{N-m+1} \sum_{i=1}^{N-m+1} \ln C_i^m(r) \quad (4)$$

170 2) By increasing the dimension from m to $m+1$ and repeating steps 2~4, $H^{m+1}(r)$ can be
 171 obtained.

172 3) The definition of the ApEn can be given as:

$$173 \quad ApEn(m, r) = \lim_{N \rightarrow \infty} [H^m(r) - H^{m+1}(r)] \quad (5)$$

174 If N is finite, formula 5 is rewritten as:

$$175 \quad ApEn(m, r, N) = H^m(r) - H^{(m+1)}(r) \quad (6)$$

176

177 **Multiscale approximate entropy**

178 To improve upon ApEn, the multiscale approximate entropy (MApEn) based on ApEn
 179 has been proposed to improve the robust and accuracy of model. Furthermore, the MApEn
 180 algorithm, overcomes the limitations of ApEn [17]. Interestingly, compared with only one
 181 feature obtained by ApEn, these MApEn values reflected by different scales are able to be used
 182 as a cluster of classification parameters for the subsequent SVM training model. The concrete
 183 steps of the MApEn algorithm are as follows [17]:

184 1) Assume the initial discrete series is $X = \{x(i), i = 1, 2, \dots, N\}$, and its length is N .

185 2) Construct a coarse time series $\{z^{(\tau)}\}$, where τ represents the scale factor, and then, the
 186 scaling time series can be expressed as:

$$187 \quad z^\tau(j) = \frac{1}{\tau} \sum_{i=(j-1)\tau+1}^{j\tau} x(i) \quad 1 \leq j \leq N/\tau \quad (7)$$

188 Equation 7 is the same as the original sequence provided that the scale factor $\tau=1$.
189 Furthermore, each coarse-graining series can be regarded as evenly dividing the original series,
190 and each segmentation length is τ .

191 By combining multiscales with the approximate entropy to generate MApEn, the MApEn
192 algorithm is able to characterize the nonlinear information of series more effectively. Fig. 4
193 exhibits the detailed flowchart.

194 **Fig. 4. Flowchart of Multiscale Approximate Entropy Algorithm.**

195

196 **MApEn algorithm and its performance**

197

198 **Fast ApEn algorithm and setting parameters**

199 First, we can calculate the ApEn according to the abovementioned equations 2~6. There
200 is plenty of redundant computing in some steps; however, it is time-consuming and cannot be
201 used for real-time determination. Bo et al. [18] proposed a type of fast ApEn algorithm that can
202 shorten the running time by nearly 5 times. The main steps are as follows:

203 First step: The distance matrix $D(N \times N)$ for the initial N points time sequence is
204 calculated, and the element in the i^{th} row and j^{th} column can be denoted as d_{ij} . The rules for
205 calculating d_{ij} are based on the following algorithm:

$$206 \quad d_{ij} = \begin{cases} 1 & |x(i) - x(j)| < r \\ 0 & |x(i) - x(j)| \geq r \end{cases} \quad i = 1 \sim N; j = 1 \sim N; i \neq j \quad (8)$$

207 Second step: assuming the dimension of the pattern vector $m = 2$, we can easily obtain
208 the values of $C_i^2(r)$ and $C_i^3(r)$ using equation 9.

209
$$C_i^2(r) = \sum_{j=1}^{N-1} d_{ij} \cap d_{(i+1)(j+1)}$$

210
$$C_i^3(r) = \sum_{j=1}^{N-2} d_{ij} \cap d_{(i+1)(j+1)} \cap d_{(i+2)(j+2)} \quad (9)$$

211 Third step: According to the values of $C_i^2(r)$ and $C_i^3(r)$, then we get $H_2(r)$ and $H_3(r)$.

212 Fourth step: The ApEn value can be calculated by equations 5~6.

213 Four parameters are involved in the MApEn algorithm: the length of the input signal N ,
214 the dimension of the pattern vector m , the similar tolerance threshold value r , and the time
215 scale factor τ . For the ApEn algorithm, choosing the right parameters is of extreme importance
216 to the algorithm.

217 After simulating several experiments, we finally select $N = 1500, m = 2, r = 0.12 \times STD$ as
218 our experimental parameters, where STD represents the standard deviation of initial time series.
219 The ApEn values of the UWL signal of the two types of wheat at different tolerance thresholds
220 were simulated using Matlab 2018a, and the results are shown in Fig. 5. As shown in Fig. 5, the
221 ApEn values of the two types of wheat vary depending on different tolerance thresholds r .
222 Although the ApEn values of the two types of wheat are small, the differences between the
223 healthy and mouldy wheat are obvious based on the ApEn values, where r varies from 0.1 to
224 0.19. In addition, another conclusion from the experimental results is that the smaller ApEn
225 value of the mouldy wheat reflects that the activities of *Aspergillus* fungi are more regular and
226 intensive than the healthy wheat itself, and thus, the value can be used as a classification feature
227 to recognize mouldy wheat.

228 **Fig. 5. ApEn Values for Different Tolerance Thresholds of UWL Signals of Healthy and**
229 **Mouldy Wheat.**

230 **Discussions**

231

232 **Performance analysis of the MApEn algorithm**

233 The ApEn algorithm only offers one classification feature; therefore, in order to
234 overcome this shortcoming and get more classification feature values, the MApEn algorithm is
235 introduced in this paper. For ApEn algorithm, the parameters $N = 1500, m = 2, r = 0.12 \times STD$ are
236 finally chosen and simulated via experiments. In addition to the parameters mentioned above, the
237 scale factor τ is a decisive factor in the performance of the MApEn algorithm. Due to the limited
238 length of the initial time series, τ is usually assigned a value from 2 to 10. The curve of the
239 MApEn value at different scale factors is shown in Fig. 6.

240 **Fig. 6. MApEn Values for Different Scale Factors of UWL Signals of Healthy and Mouldy** 241 **Wheat.**

242 Observing Fig. 6, the following conclusions can be achieved:

- 243 ① The MApEn values of the UWL of the two types wheat sample shows an inverse trend;
244 ② Compared with ApEn, the MApEn algorithm can offer several classification features that
245 can be used at the same time under different scales rather than only one feature gained by
246 ApEn algorithm.

247

248 **Bipartition classification and performance assessment by SVM**

249 To solve the classification problem between healthy and mouldy wheat, the SVM is
250 introduced in this work. The SVM, proposed by Cortes and Vapnik [16] in 1995, is a type of
251 linear classifier based on classification boundaries. Computationally, the striking points of the

252 SVM are how to choose the penalty and kernel parameters, and the kernel parameter impacts the
253 nonlinear transformation of the input feature space from a lower-dimensional to a higher-
254 dimensional space. In other words, this problem can be considered to be an optimization problem
255 in which we seek to help the kernel function to find the optimal plane, by which we can conduct
256 linearly separated classification based on a nonlinear transformation [19]. Although the training
257 samples are not large enough, the SVM can achieve a good classification performance [20].
258 Currently, the SVM has become one of most widely used learning algorithm, and it has been
259 applied in various fields [21,22].

260 Based on the SVM method and the purpose of the classification, the three parameters in
261 Table 1 and the ApEn value act as the classification features. The UWL signals of total groups of
262 the two types wheat kernels have been trained, and then, the abovementioned 120 healthy and
263 mouldy wheat samples are separately used as the testing group. Adopting the SVM training
264 model offered by Lin's group from Taiwan University, the main parameters of the SVM are set
265 as follows. The type of kernel function is a radial basis function, and the error value that
266 terminates the iteration is 0.001. The ROC curve represents the classification result and is
267 illustrated in Fig. 7, where the blue curve represents the classification performance of the
268 MApEn algorithm, and the red curve represents the classification performance of the ApEn
269 algorithm.

270 **Fig. 7. The ROC Curves of Two Classification Models.**

271 From the ROC curves, Tables 2 and 3 can be calculated, where AUC, S.E., C.I., and PA
272 represent the area under the curve, the standard error of the area, the confidence interval and the
273 performance of the classifier, respectively. Comparing Table 2 with Table 3 shows that the
274 classification accuracy rate based on MApEn has been improved obviously. In addition, the

275 standard error decreases by introducing the MApEn algorithm. The experimental results validate
276 that the MApEn values can act as a cluster of main classification features to recognize wheat
277 kernels as healthy or mouldy.

278 **Table 2. Classification Result Using ApEn as the Main Classification Feature.**

AUC	S.E.	95% C.I.	PA
0.8693	0.0272	[0.8260 0.9226]	Good

279 **Table 3. Classification Result Using MApEn as the Main Classification Features.**

AUC	S.E.	95% C.I.	PA
0.8874	0.0246	[0.8392 0.9356]	Good

280

281 **Conclusions**

282 The UWL signals from different conditions of wheat kernels can reflect their inner
283 physiological and pathological changes; therefore, it can be used as an environmentally friendly
284 and nondestructive method to assess wheat quality. Since the UWL signal is so sensitive to
285 environmental factors and the inner states of wheat kernels, further studies and experiments
286 seeking to minimize these influences caused by these factors need to be conducted.

287 Multiscale approximate entropy is introduced to analyse the UWL signals in this paper.
288 Subsequently, we have used an SVM to establish the classification model. The results of the
289 simulations via an experiment show that the MApEn algorithm is efficient and effective at
290 analysing random UWL signals. One main deficiency is that we only establish a binomial
291 classification model in this work due to the limited experimental data, and the MApEn algorithm
292 fails to exhibit its advantages. Furthermore, recognizing mouldy wheat kernels is a continuous
293 process during their storage period; therefore, establishing a multiclassification model to classify
294 and recognize the degree of mould is of extreme significance to help the operators to acquire

295 accurate information about the degree of mould and make scientific choices, which requires
296 further research to improve the precision of the established model.

297

298 **Acknowledgements**

299 The authors are grateful for all the reviewers and the editor for their valuable suggestions
300 and comments.

301

302 **References**

- 303 1. USDA. Grain: world markets and trade. United States: Department of Agriculture
304 Foreign Agricultural Service; 2018.
- 305 2. CHYXX. 2019. Available from: <https://www.chyxx.com/industry/201910/793702.html>.
- 306 3. Milani J. Ecological conditions affecting mycotoxin production in cereals: a review. *Vet*
307 *Med.* 2013;58: 405-411.
- 308 4. Heshmati A, Zohrevand T, Khaneghah AM, Nejad ASM, Sant'Ana AS. Co-occurrence of
309 aflatoxins and ochratoxin A in dried fruits in iran: dietary exposure risk assessment. *Food*
310 *Chem Toxicol.* 2017;106: 202-208.
- 311 5. Blankson G, Mill-Robertson F. Aflatoxin contamination and exposure in processed
312 cereal-based complementary foods for infants and young children in greater Accra,
313 Ghana. *Food Control.* 2016;64: 212-217.
- 314 6. Mhiko TA. Determination of the causes and the effects of storage conditions on the
315 quality of silo stored wheat (*Triticum aestivum*) in Zimbabwe. *Nat Prod Bioprospecting.*
316 2012;2: 21-28.
- 317 7. Gurwitsch A. Die natur des spezifischen erregers der zellteilung. *Arch Mikrosk Anat*
318 *Entwicklungsmechanik.* 1923;100: 11-40.
- 319 8. Colli L, Facchini U, Guidotti G, Lonati RD, Orsenigo M, Sommariva O. Further
320 measurements on the bioluminescence of the seedlings. *Experientia.* 1955;11: 479-481.
- 321 9. Popp FA, Gu Q, Li KH. Biophoton emission: experimental background and theoretical
322 approaches. *Mod Phys Lett B.* 1994;8: 1269-1296.

- 323 10. Veselova T, Veselovsky V, Kozar V, Rubin A. Delayed luminescence of soybean seeds
324 during swelling and accelerated ageing. *Seed Sci Technol.* 1988;16: 105-113.
- 325 11. Boschi F, Basso PR, Corridori I, Durando G, Sandri A, Segalla G, et al. Weak biophoton
326 emission after laser surgery application in soft tissues: analysis of the optical features. *J*
327 *Biophotonics.* 2019;12: e201800260.
- 328 12. Nirosha J, Murugan, Nicolas Rouleau, Lukasz M, Karbowski, Micheal A, et al.
329 Biophotonic markers of malignancy: Discriminating cancers using wavelength-specific
330 biophotons. *Biochemistry and Biophysics Reports.* 2018;13: 7-11.
- 331 13. Wang Z, Wang N, Li Z, Xiao F, Dai J. Human high intelligence is involved in spectral
332 redshift of biophotonic activities in the brain. *Proc Natl Acad Sci U S A.* 2016;113: 8753-
333 8758.
- 334 14. Duan S, Wang F, Zhang Y. Research on the biophoton emission of wheat kernels based
335 on permutation entropy. *Optik.* 2019;178: 723-730.
- 336 15. Pincus SM. Approximate entropy as a measure of system complexity. *Proc Natl Acad Sci*
337 *U S A.* 1991;88: 2297-2301.
- 338 16. Cortes C, Vapnik V. Support-vector networks. *Mach Learn.* 1995;20: 273-297.
- 339 17. Costa M, Goldberger AL, Peng CK. Multiscale entropy analysis of complex physiologic
340 time series. *Phys Rev Lett.* 2002;89: 068102.
- 341 18. Bo H, Qingyu T, Fusheng Y, Tian-Xiang C. ApEn and cross-ApEn: property, fast
342 algorithm and preliminary application to the study of EEG and cognition. *Signal Process.*
343 1999;15: 100-108.
- 344 19. Chapelle O, Vapnik V, Bousquet O, Mukherjee S. Choosing multiple parameters for
345 support vector machines. *Mach Learn.* 2002;46: 131-159.

- 346 20. Zhang Y, Wu L. Classification of fruits using computer vision and a multiclass support
347 vector machine. *Sensors (Basel)*. 2012;12: 12489-12505.
- 348 21. Nagata F, Tokuno K, Mitarai K, Otsuka A, Ikeda T, Ochi H, et al. Defect detection
349 method using deep convolutional neural network, support vector machine and template
350 matching techniques. *Artif Life Robot*. 2019;24: 512-519.
- 351 22. Miyagi S, Sugiyama S, Kozawa K, Moritani S, Sakamoto SI, Sakai O. Classifying
352 dysphagic swallowing sounds with support vector machines. *Healthcare (Basel)*. 2020;8:
353 103.

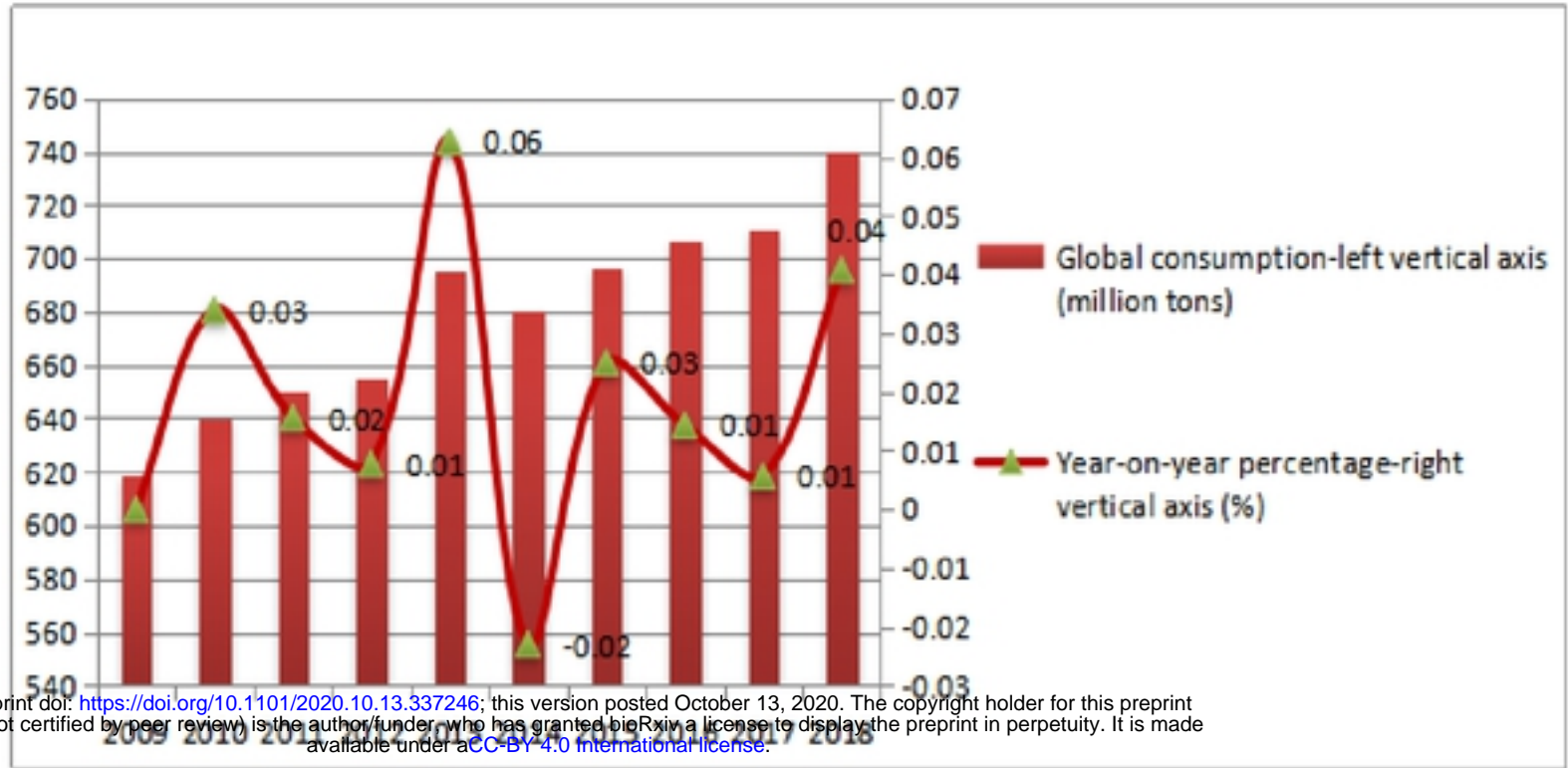


Fig. 1

bioRxiv preprint doi: <https://doi.org/10.1101/2020.10.13.337246>; this version posted October 13, 2020. The copyright holder for this preprint (which was not certified by peer review) is the author/funder, who has granted bioRxiv a license to display the preprint in perpetuity. It is made available under a [CC-BY 4.0 International license](#).



Fig. 2

bioRxiv preprint doi: <https://doi.org/10.1101/2020.10.13.337246>; this version posted October 13, 2020. The copyright holder for this preprint (which was not certified by peer review) is the author/funder, who has granted bioRxiv a license to display the preprint in perpetuity. It is made available under aCC-BY 4.0 International license.

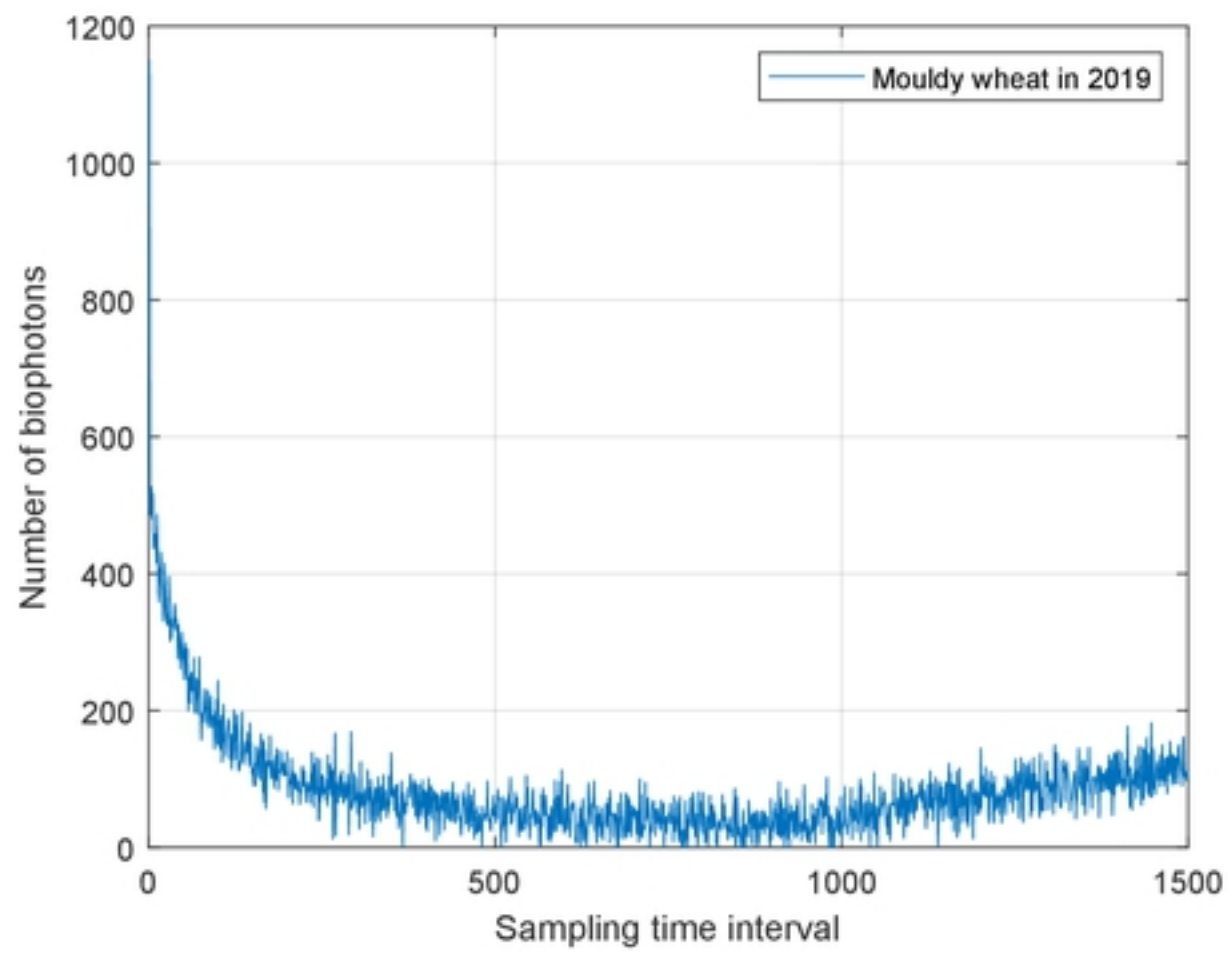
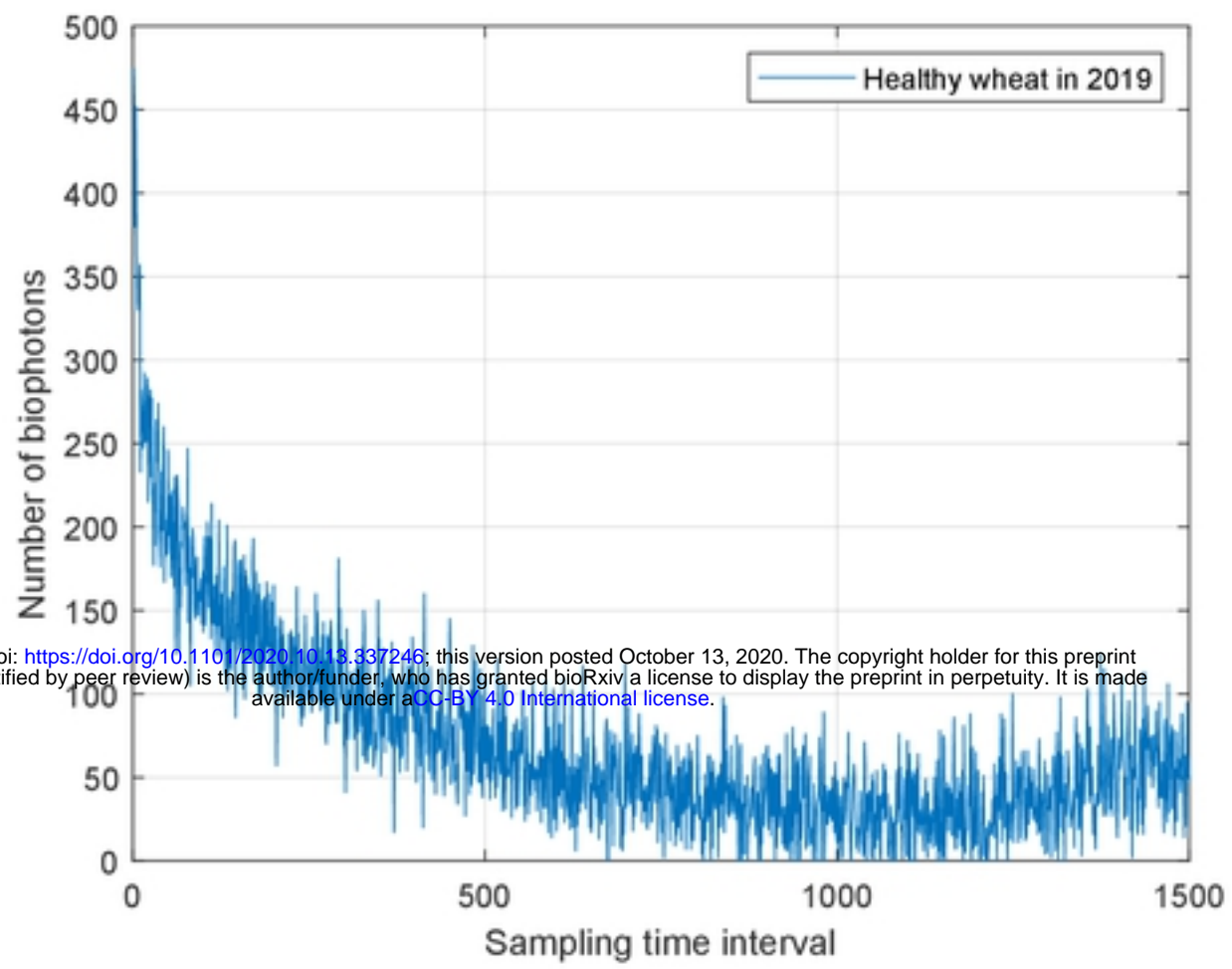


Fig. 3

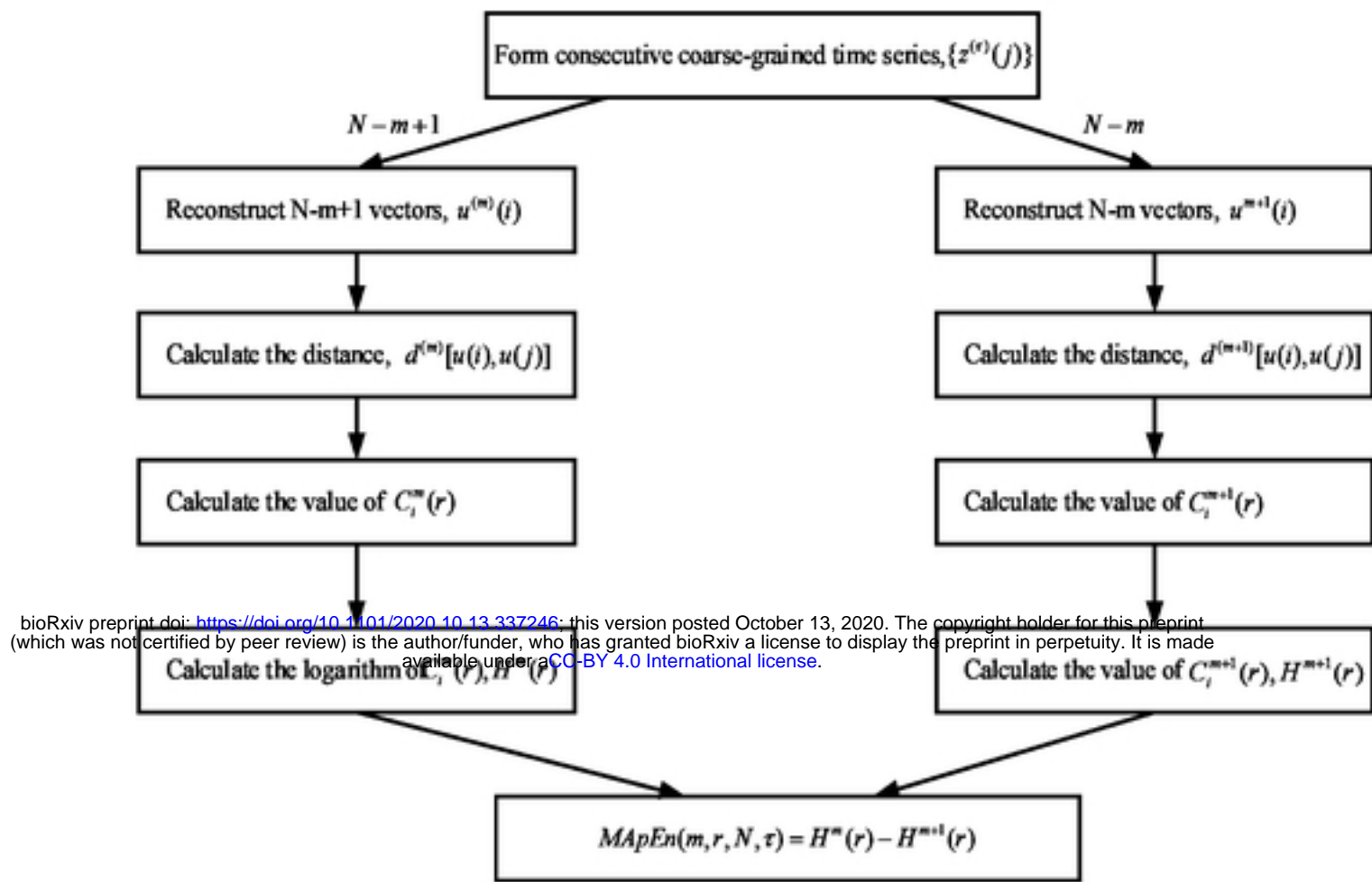


Fig. 4

bioRxiv preprint doi: <https://doi.org/10.1101/2020.10.13.337246>; this version posted October 13, 2020. The copyright holder for this preprint (which was not certified by peer review) is the author/funder, who has granted bioRxiv a license to display the preprint in perpetuity. It is made available under aCC-BY 4.0 International license.

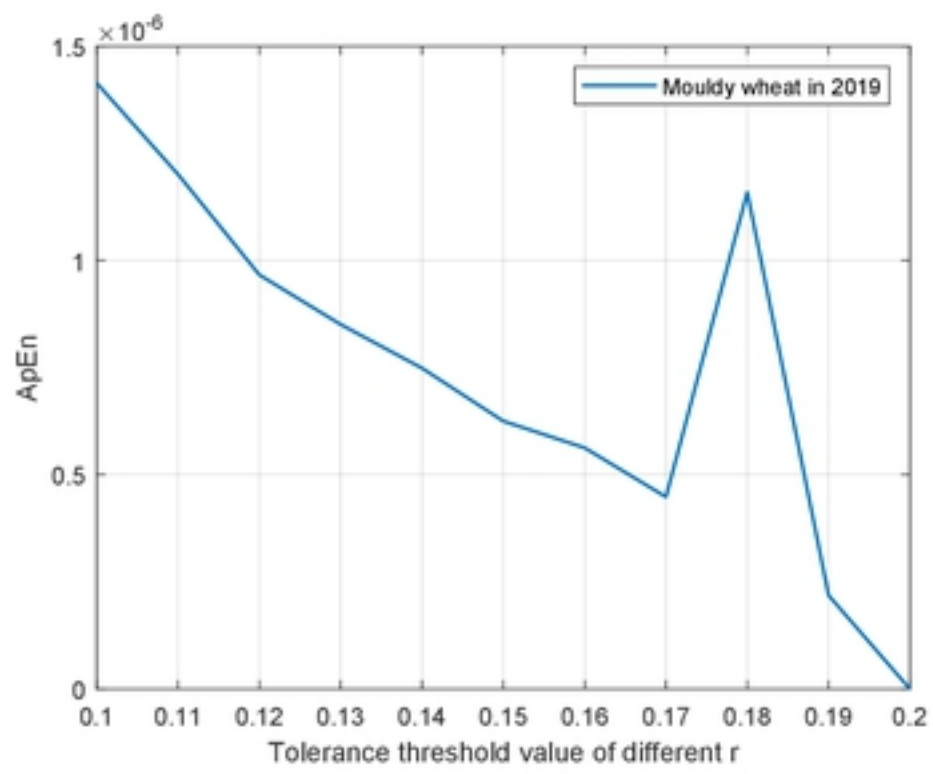
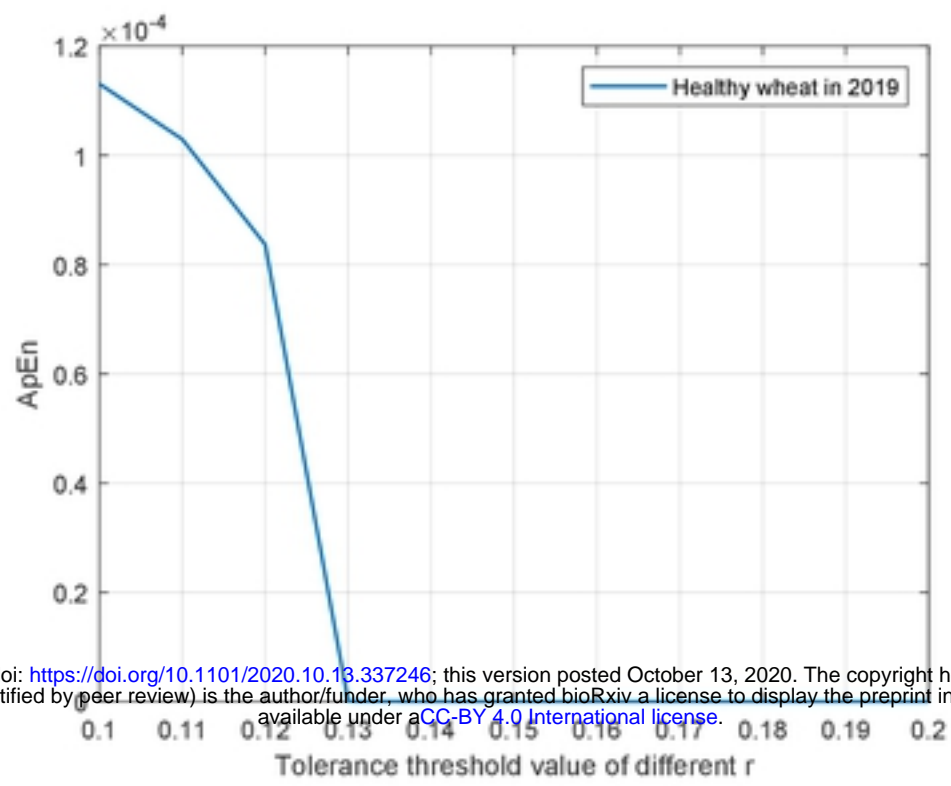
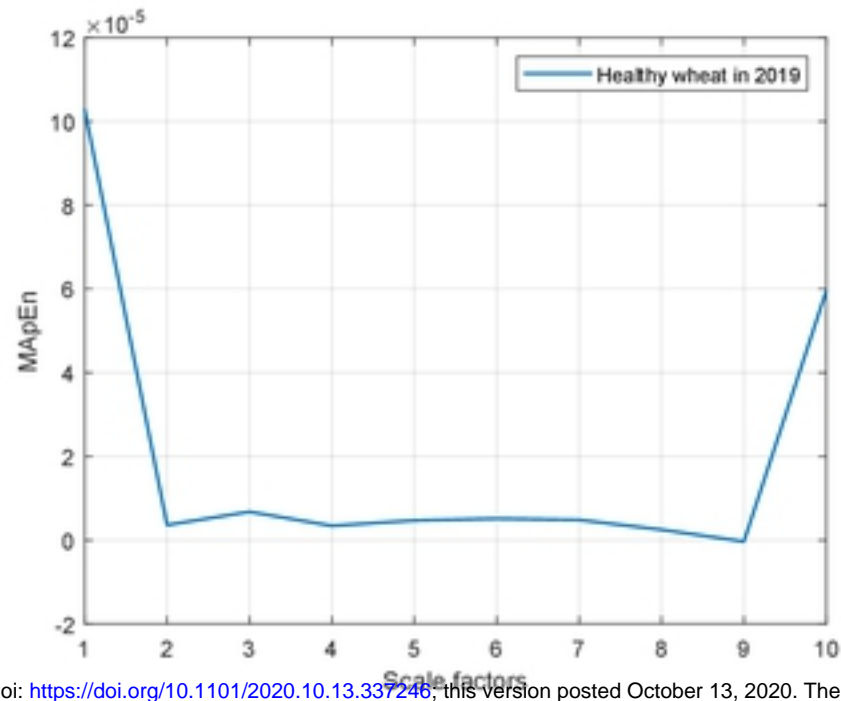


Fig. 5



bioRxiv preprint doi: <https://doi.org/10.1101/2020.10.13.337246>; this version posted October 13, 2020. The copyright holder for this preprint (which was not certified by peer review) is the author/funder, who has granted bioRxiv a license to display the preprint in perpetuity. It is made available under aCC-BY 4.0 International license.

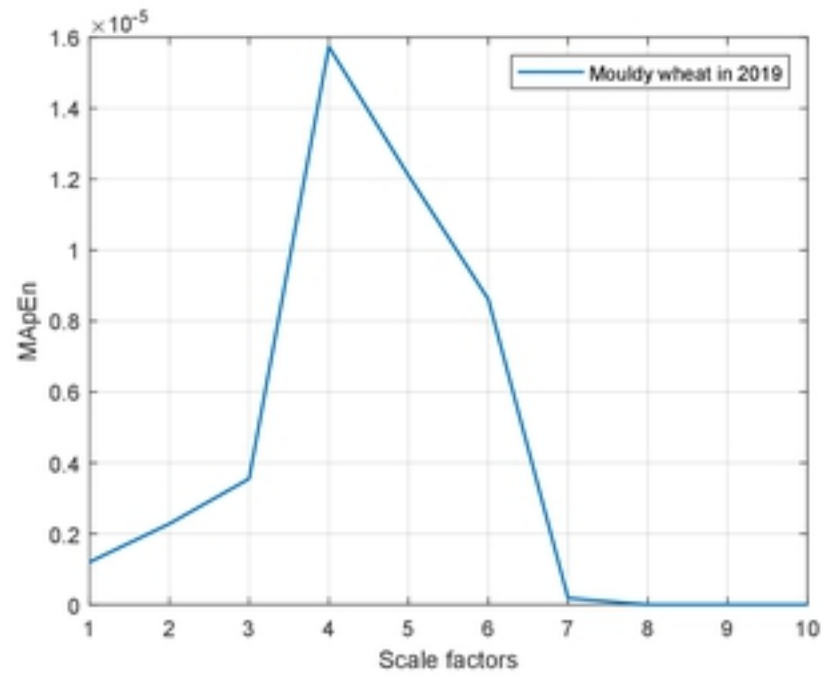
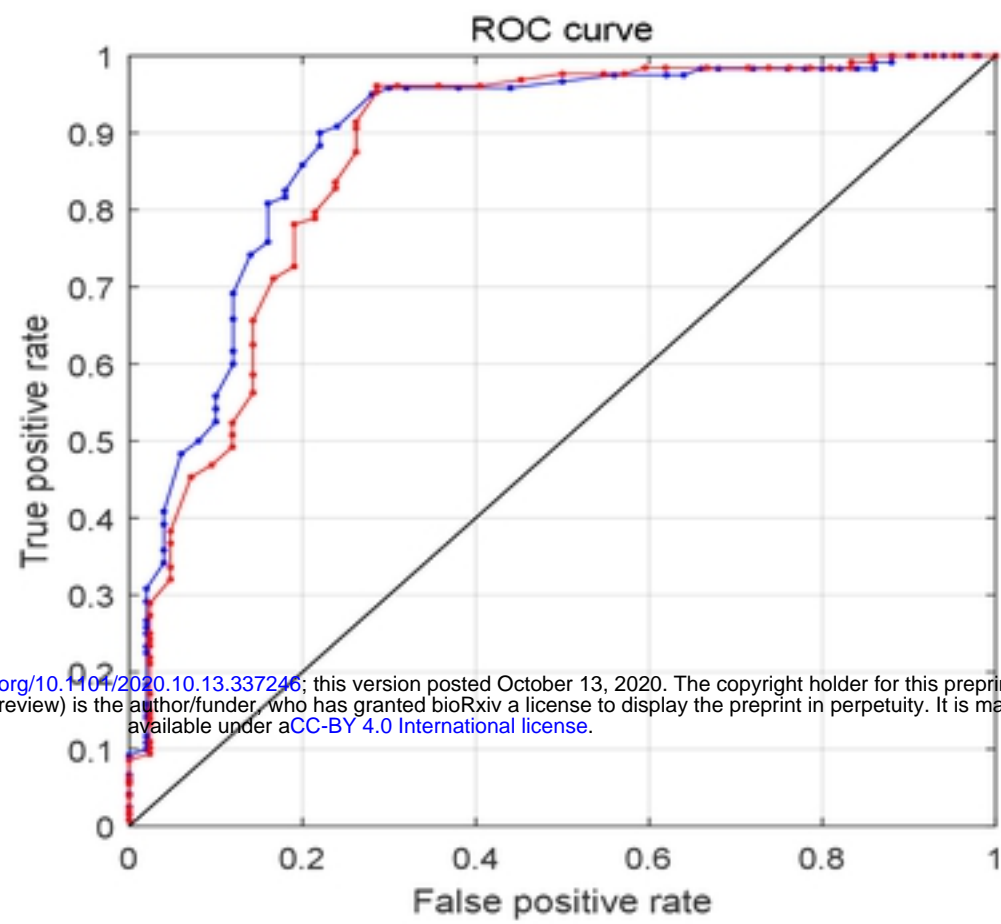


Fig. 6



bioRxiv preprint doi: <https://doi.org/10.1101/2020.10.13.337246>; this version posted October 13, 2020. The copyright holder for this preprint (which was not certified by peer review) is the author/funder, who has granted bioRxiv a license to display the preprint in perpetuity. It is made available under aCC-BY 4.0 International license.

Fig. 7